Published in final edited form as:
J Mol Biol. 2009 July 31; 390(5): 902–912. doi:10.1016/j.jmb.2009.05.062.

A Gating Model for the Archeal Voltage-Dependent K^+ Channel KvAP in DPhPC and POPE:POPG decane lipid bilayers

Daniel Schmidt, **Sam R. Cross**, and **Roderick MacKinnon**
Howard Hughes Medical Institute, Laboratory of Molecular Neurobiology and Biophysics, Rockefeller University, 1230 York Avenue, New York, New York 10065, USA.

Abstract

Voltage-dependent K^+ (Kv) channels form the basis of the excitability of nerves and muscles. KvAP is a well-characterized archeal Kv channel that has been widely used to investigate many aspects of Kv channel biochemistry, biophysics and structure. In this study a minimal kinetic gating model for KvAP function in two different phospholipid decane bilayers is developed. In most aspects KvAP gating is similar to the well-studied eukaryotic Shaker Kv channel: conformational changes occur within four voltage sensors followed by pore opening. Unlike Shaker, KvAP possesses an inactivated state that is accessible from the pre-open state of the channel. Changing the lipid composition of the membrane influences multiple gating transitions in the model, but most dramatically the rate of recovery from inactivation. Inhibition by the voltage sensor toxin VSTx1 is most easily explained if VSTx1 binds only to the depolarized conformation of the voltage sensor. By delaying the voltage sensor's return to the hyperpolarized conformation VSTx1 favors the inactivated state of KvAP.

Keywords

Kv channel; voltage-dependent gating; channel-inactivation; voltage sensor toxin; lipid membrane

Introduction

Voltage-dependent ion channels are channels whose gating is controlled by the cell's membrane voltage. Depolarization-activated voltage-dependent channels, for example, exhibit a low open probability when the cell membrane voltage is near its resting value, typically −60 mV to −100 mV (inside relative to outside), and exhibit a high open probability at more depolarized membrane voltages, for example 0 mV. The ability of voltage-dependent channels to gate as a function of membrane voltage permits the propagation of nerve impulses known as action potentials [1]. Voltage-dependent ion channels are interesting proteins not only because they produce electrical signals in living cells, but also because the process of protein conformational control by a transmembrane electric field is fascinating in its own right.

For historical reasons the most complete information on the function of voltage-dependent channels comes from studies of eukaryotic channels that produce electrical signals in neurons [2] (change this reference to the Hodgkin Huxley 1952 papers). The most detailed models have

Correspondence: mackinn@rockefeller.edu.

been developed for voltage-dependent K^+ (Kv) channels, particularly the Shaker channel [3; 4; 5; 6]. According to the models, upon membrane depolarization the four voltage sensors of the Shaker channel each undergo a conformational change detectable as a transient gating current resulting from the motion of charged amino acids within the membrane electric field. The degree to which voltage sensor conformational changes are independent is not entirely certain, but the data are explicable if the movements are essentially independent [4; 5]. After the voltage sensors move from their hyperpolarized to their depolarized conformation the pore then opens in a concerted manner, at which time ions begin to conduct. Because multiple transitions must occur (multiple voltage sensor conformational changes followed by pore opening) ion conduction in the Shaker channel turns on with a sigmoid-shaped time course following membrane depolarization [6]. After Shaker channels open they spontaneously 'inactivate' even if the membrane remains at the depolarized voltage. Inactivated channels no longer conduct ions, but inactivation does not represent a return to the original closed conformation: the voltage sensors remain in a depolarized conformation (or nearly so) and the pore's gate remains open, however, it becomes plugged by the N-terminus, which acts as a blocker of the ion permeation pathway [7]. If the N-terminus is truncated inactivation is slowed but not eliminated. The remaining inactivation, which is independent of the N-terminus and is not well understood at a mechanistic level, is termed C-type inactivation [8]. Most Kv channels undergo C-type inactivation, or some form of inactivation that is independent on the N-terminus, to some degree.

In recent years Kv channels have been discovered in the most unlikely organisms. It was assumed that prokaryotes would have no use for Kv channels: we still do not understand why certain prokaryotes have them, but it is clear that they do. A Kv channel called KvAP from the thermophilic Archaea *Aeropyrum pernix* yielded the first atomic structural information on any voltage-dependent channel [9]. The KvAP channel, which can be synthesized by *E. coli* and is biochemically robust, has become a focus of study in many laboratories. It is known to open upon membrane depolarization, inactivate, and interact with well-known Kv channel toxins [10; 11]. The purpose of the present study is to develop a model for gating through which KvAP can be compared to the better-studied eukaryotic Kv channels such as the Shaker channel.

Results

The relationship between activation and inactivation

Figure 1A shows K^+ current carried by KvAP channels during a voltage protocol consisting of two sequential membrane-depolarizing steps separated by a short time interval at the holding voltage. During the first step, following the capacitive transient, channels open with a sigmoid-shaped time course, reach a maximum, and then visibly begin to inactivate. Channels behave similarly during the second depolarizing step except that the total number of active channels (and thus the amount of current) is reduced (Figure 1A, separation between dashed lines). The Shaker K^+ channel (an N-terminal inactivation-removed version) exemplifies the more typical Kv channel response to a similar voltage protocol: the current level at the start of the second step is roughly equal to the current level at the end of the first (Figure 1B, dashed line). This is because channels that inactivate during the first depolarizing step do not have sufficient time to recover before the second step and are therefore still inactivated. The unusual aspect of KvAP is that there are fewer active channels in the second step than were present at the end of the first. Other differences between the KvAP and Shaker channels reflect mainly differences in the rates of channel opening and inactivation. For example, the sigmoid-shaped opening observed in the KvAP traces occurs too rapidly in Shaker channels to be observed in the recordings shown here.

Why for KvAP are fewer active channels observed in the second pulse than at the end of the first? This observation is explicable if KvAP can open or inactivate rather than open and then

subsequently inactivate. To elaborate, if upon membrane depolarization channels move sequentially from closed to open to inactivated according to the scheme

$$C \leftrightarrows O \leftrightarrows I \tag{1}$$

then the fraction of open channels in the second step can never be smaller than at the end of the first. If, on the other hand, channels can either open or inactivate according to the scheme

$$\begin{array}{ccc} C & \leftrightarrows & O \\ \downarrow & & \\ I & & \end{array} \tag{2}$$

then the fraction of open channels can be smaller in the second step than at the end of the first. In fact, given a sufficiently brief time interval between steps and sufficiently brief steps the second scheme predicts that the fraction of initial current (n = 0 step) remaining in the n^{th} step will be given by

$$\frac{I_n}{I_0} = A^n \tag{3}$$

where A, a constant, is a function of the rate constants. Figure 2A shows the current elicited by a series of four steps n=0 to 3; Figure 2B graphs the fraction of initial current (n = 0) remaining as a function of step number n. The solid curve shows equation (3) fit to the data. From this simple analysis we conclude that KvAP, upon membrane depolarization, can either open or inactivate directly from a closed conformation.

A minimal scheme for KvAP gating

In order to account for the sigmoid-shaped time course of opening we considered a modified version of scheme (2)

$$\begin{array}{ccc} (C_0 \leftrightarrows C_1)^4 & \bullet & \leftrightarrows O \\ & \downarrow\uparrow & \\ & I & \end{array} \tag{4}$$

in which the closed state C is replaced by a pair of connected closed states, C_0 and C_1, raised to power 4. The basic idea, which has been expressed in different ways in other descriptions of Kv channel gating, is that the voltage sensors must first undergo a conformational change before the pore can open [3; 4; 5; 6]. Scheme (4) invokes the atomic structure of Kv channels, which features a single central pore surrounded by four identical voltage sensor domains. The voltage sensors are each attached to the pore but they do not contact each other directly. Scheme (4) assumes that each of the four voltage sensors can independently undergo a conformational change $C_0 \leftrightarrows C_1$, and then once all four sensors have achieved the C_1 conformation – a 'pre-open' state signified by a dot in the scheme – the channel can either open or inactivate. This scheme is obviously an over simplification of a much more complex molecular process, but to what extent can it approximate the behavior of KvAP under various voltage protocols?

All of the experiments have been carried out in planar lipid bilayers with 150 mM KCl in the internal and external solutions. Figure 3 shows examples of raw current traces as well as graphs of quantities extracted from multiple current measurements for a set of conventional voltage protocols. Smooth solid curves correspond to the model prediction, with rate constants (k_0)

and degree of voltage-dependence (z) for each step, derived through global fitting, shown in Figure 3A.

Voltage dependence of gating is evident in the activation curve (Figure 3B), in the rate of closure when the membrane is returned to its holding voltage (deactivation) (Figure 3C), in the rate of recovery from inactivation (Figure 3E), in the voltage dependence of steady state inactivation (Figure 3F), and in the fraction of channels that inactivate after a given time as a function of voltage (Figure 3G). Fits of the six rate constants and their voltage dependence suggest that all transitions exhibit some degree of voltage dependence, with the strongest in the $C_0 \leftrightarrows C_1$ transitions. The existence of some voltage dependence in the transition between the pre-open state and the open state gives rise to a continued increase of current after an initial plateau in the activation curve (Figure 3B). The very strong voltage dependence in the $C_0 \leftrightarrows C_1$ transition occurs mostly in the $C_1 \rightarrow C_0$ direction. According to the model this accounts for the strong voltage dependence in the rate of deactivation (Figure 3C). Such asymmetry in the distribution of voltage dependence over a forward and backward reaction is common and does not imply that the reaction necessarily follows a different pathway in the two directions. The asymmetry is explicable if the transition state is offset to one side of the reaction pathway, in this case toward C_0.

The inactivation process is also voltage dependent, especially in the $I \rightarrow C_1$ transition. This voltage dependence is directly observable in the voltage protocol to study the rate of recovery from inactivation (Figure 3E). We note that scheme (4) can account for the inactivation observed during a depolarizing step (Figure 3D) even though there is no direct connection between the open and inactivated states. This is because the model permits the channel to transition back and forth between the opened and the pre-opened state. From the pre-opened state the channels can enter the inactivated state, which ultimately acts as a sink. Thus, according to the model, inactivation observed during a depolarizing step represents channels transiting from O to pre-opened to I. These data do not demonstrate the absence of a direct connection between O and I. They simply indicate that given the currently available data it is not necessary to invoke such a connection.

A subtle feature of the voltage-dependence of inactivation is also compatible with the absence of a direct connection between O and I. Figure 3G presents in greater detail data from series of depolarizing steps, similar to Figure 2. The graph in the middle of Figure 3G shows the fraction of remaining current as a function of step number for series of depolarizing steps of different duration. The data are fit to exponential functions of step number. The graph on the right shows one minus the exponential base, which approximates the fraction of inactivation in successive steps of the series as a function of step duration. Two curves are for step depolarization voltages of 20 mV (filled circles) and 100 mV (empty circles). For short duration steps the 100 mV depolarization causes a larger fraction of channels to inactivate (inset). This is easy to understand in terms of scheme (4) because at 100 mV the voltage sensors transit from C_0 to C_1 more rapidly, causing channels to achieve the pre-open state from which they can inactivate. As the step duration is lengthened, however, the curves cross over, meaning fewer channels inactivate at 100 mV compared to 20 mV. This observation seems to suggest that channels are relatively protected from inactivation when the open state is favored by strong depolarization.

Lipid dependence of gating

KvAP gating has been shown to depend on properties of the lipid membrane [12]. The experiments described in this study so far were carried out using planar bilayers formed from Diphytanolycholine (DPhPC). Figure 4 shows the current response to the same voltage protocols described in Figure 3 but in membranes formed from Phosphatidylethanolamine (POPE) and Phosphatidylglycerol(POPG) at a ratio of 3 to 1. The currents in POPE:POPG

membranes are qualitatively similar, but there are quantitative differences. For example, channels activate at more negative voltages and the shape of the activation curve is somewhat different (Figure 3B and Figure 4B). The inactivation observed during a depolarizing step occurs at a slower rate (Figure 3D and Figure 4D) and the curve describing the time constant for recovery from inactivation is shifted to more negative voltages in the POPE:POPG membranes (Figure 3E and Figure 4E). This latter effect is manifest in the tables of rate constants as a significantly smaller rate constant for exit out the inactivated state in POPE:POPG membranes (Figure 3A and Figure 4A). The practical consequence of this difference is that it is much easier to study KvAP channels in DPHPC membranes: at a holding voltage of −100 mV recovery following a depolarizing step requires 10 seconds in DPhPC and 90 seconds in POPE:POPG.

States accessible to the voltage sensor toxin VSTx1

Voltage sensor toxins from tarantula venoms inhibit Kv channels by partitioning into the outer leaflet of the cell membrane and binding in a reversible manner to the voltage sensor paddle [10; 13; 14; 15; 16]. In binding to the voltage sensor paddle voltage sensor toxins modify Kv channel gating. One type of voltage sensor toxin called VSTx1 inhibits KvAP channels [10; 11]. When VSTx1 is applied the K^+ currents are reduced as shown (Figure 5A,B).

The graph in Figure 5C plots the fraction of uninhibited KvAP channels as a function of the VSTx1 concentration. This appears to be a reasonably standard titration curve except that at high toxin concentrations the uninhibited fraction does not approach zero. The reason for incomplete inhibition at high VSTx1 concentrations is that a fraction of the channels become uninhibited during the interval between depolarizing steps. Figure 5D shows this effect of recovery from inhibition in a graph of the ratio of currents (I/I_{max}) in a pair of depolarizing steps as a function of the intervening time duration (Δt) at the holding voltage. Two curves correspond to the absence (squares) and presence (circles) of a constant concentration of VSTx1. When the two depolarizing steps are closely spaced the second pulse has less current. As the steps are spaced further apart the current in the second step approaches that in the first. This behavior is qualitatively similar to the inactivation observed in KvAP in the absence of VSTx1 (Figure 1A and Figure 2). Inactivation is not observed even at the shortest time interval in the absence of VSTx1 in Figure 5D because at −120 mV (the holding voltage in this experiment) in DPhPC the time constant for recovery from inactivation is very brief (Figure 3E).

Figure 5E shows that a high concentration of VSTx1 has almost no effect over a time period of 600 seconds as long as the channels are held closed by negative membrane voltage (i.e. the first depolarizing step after a 600 second exposure to VSTx1 has close to control levels of current). Following a single depolarizing step, however, nearly all channels are inhibited on subsequent depolarizing steps. The inhibition is completely reversible: if after inhibition the membrane is held at a negative voltage for a sufficiently long period of time the channels recover completely (Figure 5F).

These effects of VSTx1 on KvAP channels are compatible with two possible interpretations. A first interpretation is that VSTx1 binds to the voltage sensors independent of whether they are hyperpolarized or depolarized, and by binding the toxin stabilizes the inactivated state. For example, a KvAP channel with VSTx1 attached to its voltage sensors might have an increased rate into or a decreased rate out of the inactivated state. A second interpretation is that VSTx1 follows a simple rule: that it can bind to voltage sensors only when they are in a depolarized conformation. All of the properties described in Figure 5 would follow naturally from this rule because amongst the states associated with depolarized voltage sensors the inactivated state is the most stable. Thus, by binding to the voltage sensor paddle VSTx1 would capture the voltage

sensor depolarized, delay its return to the hyperpolarized conformation, and thereby prolong inactivation.

Figure 5G shows that when the residual uninhibited current in the presence of VSTx1 (or the current that has recovered from inhibition by holding the membrane voltage negative in the presence of VSTx1, as in Figure 5F) is superimposed on traces recorded prior to the addition of VSTx1 they are kinetically indistinguishable. The voltage-activation curves are also the same (Figure 5H). The simplest explanation here is that the uninhibited currents are due to channels that do not have VSTx1 attached to their voltage sensors, because it seems rather unlikely that toxin-bound channels would activate and deactivate with normal kinetics. On the basis of this reasoning we think the interpretation that VSTx1 binds only to the depolarized conformation of a voltage sensor is more likely. In other words the voltage sensor paddle becomes accessible to VSTx1 upon membrane depolarization, and can return to its hyperpolarized position only after VSTx1 dissociates.

Discussion

Upon membrane depolarization a fraction of KvAP channels inactivate instead of opening. This explains why in a series of depolarizing steps separated by a short time interval the current level decreases as a function of step number; because an approximately fixed fraction of channels partition into the inactivated state with each depolarization. This gating behavior is unusual but not unique; it has been described in a number of Kv channels as well as voltage-dependent Na^+ channels [17; 18; 19; 20; 21], and it accounts for the specific electrical activity of certain neurons [19].

The KvAP gating data are consistent with scheme (4), which in over all connectivity is similar to models developed previously to describe gating of the Shaker K^+ channel [3; 4; 5; 6]. The main difference between KvAP and Shaker – which is the benchmark for analysis of Kv channel gating - is that in KvAP inactivation is connected to the pre-open state rather than the open state. Scheme (4) lends itself to a relatively simple structure-based physical interpretation. The $C_1 \leftrightarrows C_0$ transition represents the conformational changes in a voltage sensor connecting hyperpolarized and depolarized conformations. During this transition the S4 gating charges cross the membrane voltage difference. This of course is the primary step in which the electric field within the membrane directly drives the protein conformation. The pre-open state would correspond to a channel with four depolarized voltage sensors just prior to pore opening. Assuming independent voltage sensors the pre-open probability is the probability of C_1, given that the channel is not open or inactivated, to the fourth power. From the pre-open state the channel can either open or inactivate, the partition fraction being determined by the relative magnitudes of $k_{\bullet\rightarrow O}$ and $k_{\bullet\rightarrow I}$. During a sustained depolarizing step channels slowly inactivate through the sequence $O \leftrightarrows \bullet \rightarrow I$ I is the lowest energy state given four depolarized voltage sensors and therefore channels eventually inactivate completely, or nearly so, with a sufficiently long depolarizing step.

This description of KvAP gating can explain the observed effects of VSTx1 if the toxin can bind only to the depolarized conformation of the voltage sensor, a conclusion that is strongly supported by the data in Figure 5. Not only does it appear that the toxin cannot associate with a voltage sensor until the depolarized conformation is achieved, but the data also suggest that the voltage sensor cannot return to the hyperpolarized conformation until VSTx1 dissociates. This situation causes VSTx1 to effectively capture the voltage sensors in their depolarized conformation. This ultimately will favor inactivation because the inactivated state is the lowest energy conformation available to a channel with four depolarized voltage sensors.

What conformation of KvAP does the inactivated state represent? We do not yet know the answer to this question for KvAP, or in fact with certainty for any Kv channel undergoing inactivation mediated by a mechanism other than occlusion of the pore by the N-terminus (ball and chain inactivation)[8]. In the Shaker channel the C-type inactivated state is associated with a change in the reactivity of cysteine residues substituted at certain locations near the selectivity filter[22]. This observation has led to the proposal that a conformational change of the selectivity filter underlies C-type inactivation in Shaker[23]. Studies of gating in Kv2.1 and Kv3.1 show that these channels can inactivate from pre-open states and the open state by a mechanism that is thought to be distinct from C-type inactivation in Shaker[21,24]. It is likely that inactivation occurs through different physical mechanisms in different Kv channels. In KvAP channels, given the extreme degree to which inactivation occurs prior to pore opening, we wonder whether inactivation could be related to the efficiency with which the voltage sensors open the pore. For example, when the voltage sensors go from hyperpolarized to depolarized the S4–S5 linkers presumably relieve their constriction on the S6 helices, which form the gate at the intracellular pore entryway, and perhaps even lift the S6 helices so they open. If the linker helices can disengage with some probability (related to the fraction of channels that successfully open) one could imagine that the gate would close even though the voltage sensors remain in a depolarized conformation. This kind of slippage mechanism would be mechanistically akin to the model proposed for desensitization in glutamate receptor channels in which activated ligand binding domains cause pore opening and then dislodge while still bound to ligand, allowing the pore to close again [24]. Further studies will be required to support or refute such a mechanism in KvAP channels.

Studies show that the function of Kv channels is very sensitive to chemical and mechanical properties of lipid membranes [12; 25; 26]. This study shows that membrane lipid composition influences several different transitions in KvAP gating. It will be interesting to understand mechanistically how different chemical components of lipid molecules – head group, glycerol backbone, ester and ether linkages, degree of saturation and structure (alkyl versus isoprenyl) of the tail – influence specific transitions in gating. Because of the extreme lipid sensitivity exhibited by Kv channels, any description of Kv channel function is only meaningful in the context of a defined membrane. The gating properties described here refer to KvAP in DPhPC-decane and POPE:POPG-decane lipid bilayers.

Material and methods

Preparation and reconstitution of KvAP channels

KvAP channel protein was expressed and purified following published procedures [10]. Gel filtration chromatography was performed using a Superdex-200 column with 100 mM KCl, 20 mM Tris-HCl pH 8.0 and 5.0 mM decyl-maltoside (DM). The eluted channel was concentrated to 10 mg/ml before reconstitution. Reconstitution was performed following a published procedure [12]. Lipids in chloroform were dried with an argon stream in a thick-walled glass tube, washed with pentane, and then placed under room vacuum for 30 minutes. Dried lipids were then hydrated with dialysis buffer containing 450 mM KCl and 10 mM HEPES-KOH pH 7.4 at a lipid concentration of 20 mg/ml. The lipid suspension was rotated at room temperature for 30 minutes and then sonicated 10–20 times (30 second each) to produce small unilamellar vesicles. Decylmaltoside (DM) was added into the vesicle suspension to a final concentration of 10 mM. The mixture was rotated for 30 minutes at room temperature and then KvAP protein was added to the lipid/detergent mixture to a protein-to-lipid ratio 0.2 (w/w). Detergent concentration was then raised to 17.5 mM. The mixture was incubated for two hours at room temperature and then dialyzed against the dialysis buffer. The buffer was changed every 12 hours. After three days the vesicles were collected, flash-frozen with liquid nitrogen, and stored at −80 °C.

Electrophysiological Recordings

The bilayer experiments followed published procedures [10]. Lipids of desired compositions were prepared by dissolving dried lipids at 20 mg/ml in decane. Lipid dissolved in decane was painted over a 300 μm hole in a polystyrene partition that separated two aqueous chambers [27]. Once formation and thinning of a planar lipid membrane was detected through monitoring of the electrical capacitance, lipid vesicles were delivered to the membrane surface with a pipette. Vesicle fusion was facilitated by the presence of a salt gradient across the membrane: 15 mM KCl on the side opposite vesicle addition (*trans* side) and 150 mM KCl on the side of vesicle addition (*cis* side). Both sides were buffered with 10 mM HEPES at pH 7.4. After vesicle fusion, the salt concentration on the *trans* side was raised to 150 mM. Voltage-clamp measurements in whole-cell mode were made using an Axopatch 200B amplifier (Axon Instruments) that was interfaced to a PC *via* a DigiData 1440A AD/DA converter (Axon Instruments). Clampex software (Axon Instruments) was used to control the hardware. The membrane current was filtered at 1.0 – 2.0 kHz and sampled at least 5.0 kHz. All voltages are reported according to electrophysiological convention, with the extracellular side of the channel taken as ground.

Kinetic modeling

Numerical modeling was performed using the Runge-Kutta integration method and the composite data were fitted for rate constants by chi-squared minimization using the Levenberg-Marquardt algorithm algorithm in Igor Pro (Wavemetrics Inc.) via custom-written procedures. For G/V, steady-state inactivation and inactivation data the residuals were derived from the linear deviation between measured and modeled data. For recovery from inactivation and deactivation data the residuals were derived from the expression [0.5 × ln(modeled values / measured values)]. All rate constants were fitted for exponential voltage dependence. The fitting errors (Fig. 3a & Fig. 4a) are estimated standard deviations of the fitting coefficients. They are based on the coefficient values one would get if the same fit was performed an infinite number of times on the same underlying data (but with different noise each time) as implement in Igor Pro.

Acknowledgments

We thank Alice L. MacKinnon for providing VSTx1 and Bruce P. Bean for discussions and advice. This work was supported by NIH Grant GM43949. D.S. was supported by the Boehringer Ingelheim Fonds. R.M. is an investigator in the Howard Hughes Medical Institute.

References

1. Hodgkin AL, Huxley AF. Resting and action potentials in single nerve fibres. J Physiol (Lond) 1945;104:176–195. [PubMed: 16991677]
2. Hodgkin AL, Huxley AF. A quantitative description of membrane current and its application to conduction and excitation in nerve. J Physiol (Lond) 1952;117:500–544. [PubMed: 12991237]
3. Hoshi T, Zagotta WN, Aldrich RW. Shaker potassium channel gating. I: Transitions near the open state. J Gen Physiol 1994;103:249–278. [PubMed: 8189206]
4. Schoppa NE, Sigworth FJ. Activation of shaker potassium channels. I. Characterization of voltage-dependent transitions. J Gen Physiol 1998;111:271–294. [PubMed: 9450944]
5. Zagotta WN, Hoshi T, Aldrich RW. Shaker potassium channel gating. III: Evaluation of kinetic models for activation. J Gen Physiol 1994;103:321–362. [PubMed: 8189208]
6. Zagotta WN, Hoshi T, Dittman J, Aldrich RW. Shaker potassium channel gating. II: Transitions in the activation pathway. J Gen Physiol 1994;103:279–319. [PubMed: 8189207]
7. Hoshi T, Zagotta W, Aldrich R. Biophysical and molecular mechanisms of Shaker potassium channel inactivation. Science (New York, N.Y.) 1990;250:533–538.

8. Hoshi T, Zagotta WN, Aldrich RW. Two types of inactivation in Shaker K+ channels: effects of alterations in the carboxy-terminal region. Neuron 1991;7:547–556. [PubMed: 1931050]

9. Jiang Y, Lee A, Chen J, Ruta V, Cadene M, Chait BT, Mackinnon R. X-ray structure of a voltage-dependent K+ channel. Nature 2003;423:33–41. [PubMed: 12721618]

10. Ruta V, Jiang Y, Lee A, Chen J, Mackinnon R. Functional analysis of an archaebacterial voltage-dependent K+ channel. Nature 2003;422:180–185. [PubMed: 12629550]

11. Ruta V, Mackinnon R. Localization of the voltage-sensor toxin receptor on KvAP. Biochemistry 2004;43:10071–10079. [PubMed: 15287735]

12. Schmidt D, Jiang QX, Mackinnon R. Phospholipids and the origin of cationic gating charges in voltage sensors. Nature 2006;444:775–779. [PubMed: 17136096]

13. Lee SY, Mackinnon R. A membrane-access mechanism of ion channel inhibition by voltage sensor toxins from spider venom. Nature 2004;430:232–235. [PubMed: 15241419]

14. Milescu M, Vobecky J, Roh SH, Kim SH, Jung HJ, Kim JI, Swartz KJ. Tarantula toxins interact with voltage sensors within lipid membranes. J Gen Physiol 2007;130:497–511. [PubMed: 17938232]

15. Swartz KJ, Mackinnon R. Mapping the receptor site for hanatoxin, a gating modifier of voltage-dependent K+ channels. Neuron 1997;18:675–682. [PubMed: 9136775]

16. Swartz KJ, Mackinnon R. Hanatoxin modifies the gating of a voltage-dependent K+ channel through multiple binding sites. Neuron 1997;18:665–673. [PubMed: 9136774]

17. Aldrich RW. Inactivation of voltage-gated delayed potassium current in molluscan neurons. A kinetic model. Biophysical Journal 1981;36:519–532. [PubMed: 6275919]

18. Aldrich RW, Getting PA, Thompson SH. Inactivation of delayed outward current in molluscan neurone somata. J Physiol (Lond) 1979;291:507–530. [PubMed: 480244]

19. Marom S, Abbott LF. Modeling state-dependent inactivation of membrane currents. Biophysical Journal 1994;67:515–520. [PubMed: 7524708]

20. Marom S, Levitan IB. State-dependent inactivation of the Kv3 potassium channel. Biophysical Journal 1994;67:579–589. [PubMed: 7948675]

21. Klemic KG, Shieh CC, Kirsch GE, Jones SW. Inactivation of Kv2.1 potassium channels. Biophysical Journal 1998;74:1779–1789. [PubMed: 9545040]

22. Yellen G, Sodickson D, Chen TY, Jurman ME. An engineered cysteine in the external mouth of a K+ channel allows inactivation to be modulated by metal binding. Biophysical Journal 1994;66:1068–1075. [PubMed: 8038379]

23. Baukrowitz T, Yellen G. Modulation of K+ current by frequency and external [K+]: a tale of two inactivation mechanisms. Neuron 1995;15:951–960. [PubMed: 7576643]

24. Klemic KG, Kirsch GE, Jones SW. U-type inactivation of Kv3.1 and Shaker potassium channels. Biophysical Journal 2001;81:814–826. [PubMed: 11463627]

25. Armstrong N, Jasti J, Beich-Frandsen M, Gouaux E. Measurement of conformational changes accompanying desensitization in an ionotropic glutamate receptor. Cell 2006;127:85–97. [PubMed: 17018279]

26. Schmidt D, Mackinnon R. Voltage-dependent K+ channel gating and voltage sensor toxin sensitivity depend on the mechanical state of the lipid membrane. Proceedings of the National Academy of Sciences of the United States of America 2008;105:19276–19281. [PubMed: 19050073]

27. Tabarean IV, Morris CE. Membrane stretch accelerates activation and slow inactivation in Shaker channels with S3–S4 linker deletions. Biophysical Journal 2002;82:2982–2994. [PubMed: 12023221]

28. Miller, C. Ion Channel Reconstitution. New York: Plenum Press; 1986.

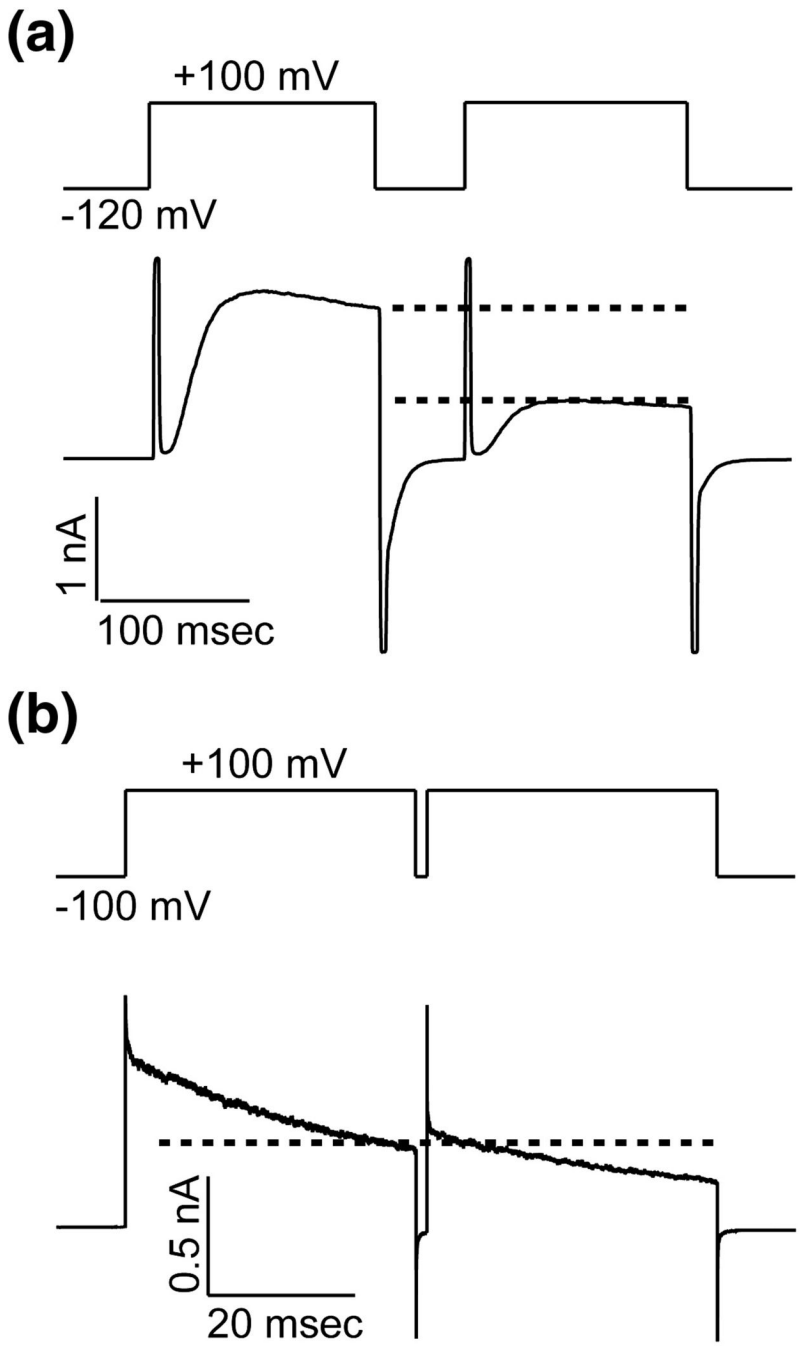

Figure 1. A Comparison of Inactivation in KvAP and Shaker Kv Channels

DPhPC vesicles containing KvAP (**A**) or Kv1.2–Kv2.1 Paddle Chimaera (**B**) were fused into DPhPC bilayers. The current response to a paired depolarization pulse from a holding voltage −120 mV (KvAP, **A**) −100 mV (Paddle Chimaera, **B**) to +100 mV was recorded. The dotted lines indicated the current levels at the end of the first and the beginning of the second depolarization pulse.

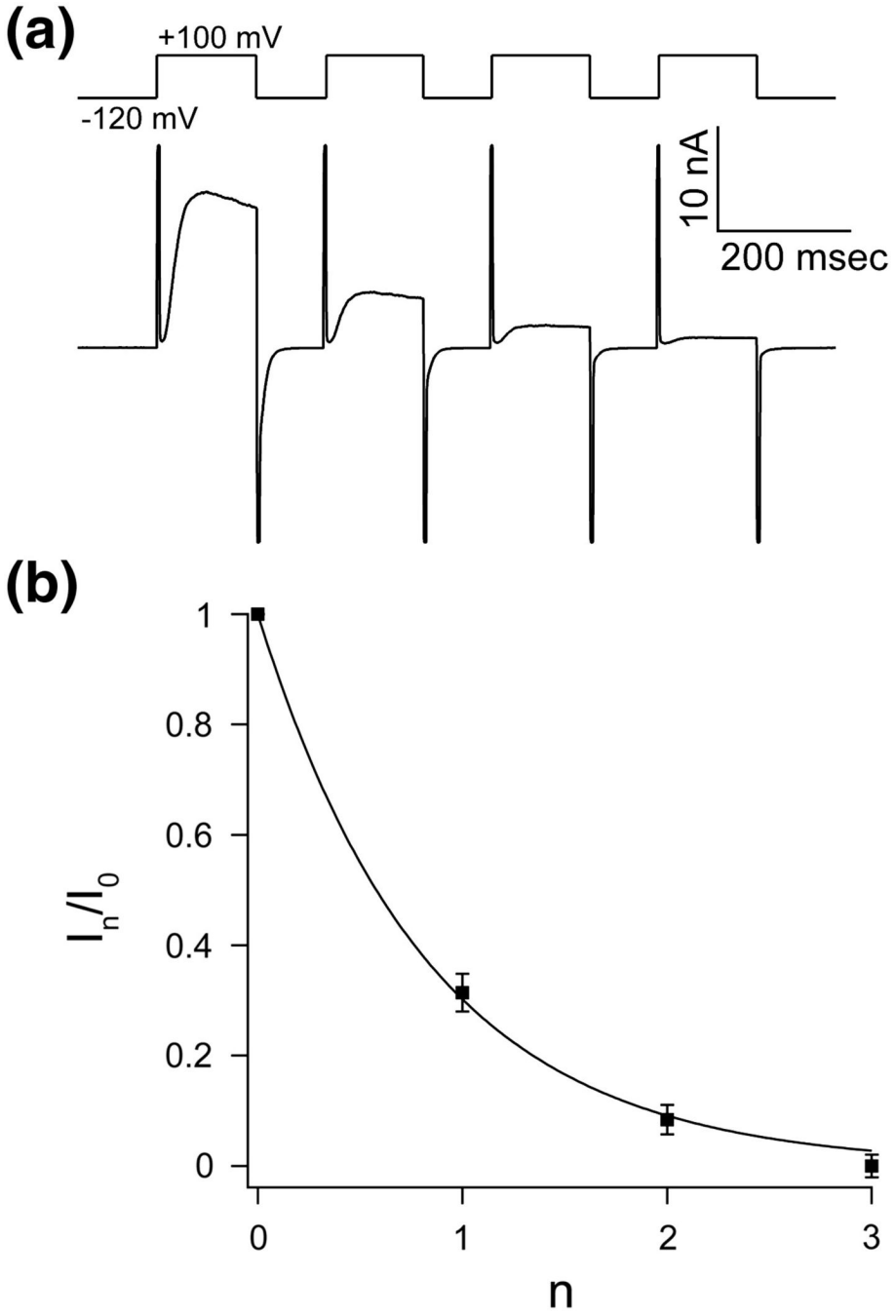

Figure 2. The accumulation of inactivation between pulses follows a geometric series

A, Repetitive pulse from holding voltage −120 mV to +100 mV. Accumulation of inactivation can be seen between pulses as a fractional decrease in current that is larger than the inactivation that occurred during the previous pulse. **B**, The fractional decrease in peak current (mean I_n/I_0 ± s.e.m, n = 5) during depolarization as function of number of pulses (n) can be fitted to a geometric progression $I_n/I_0 = A^n$ with $A = 0.302 \pm 0.01$.

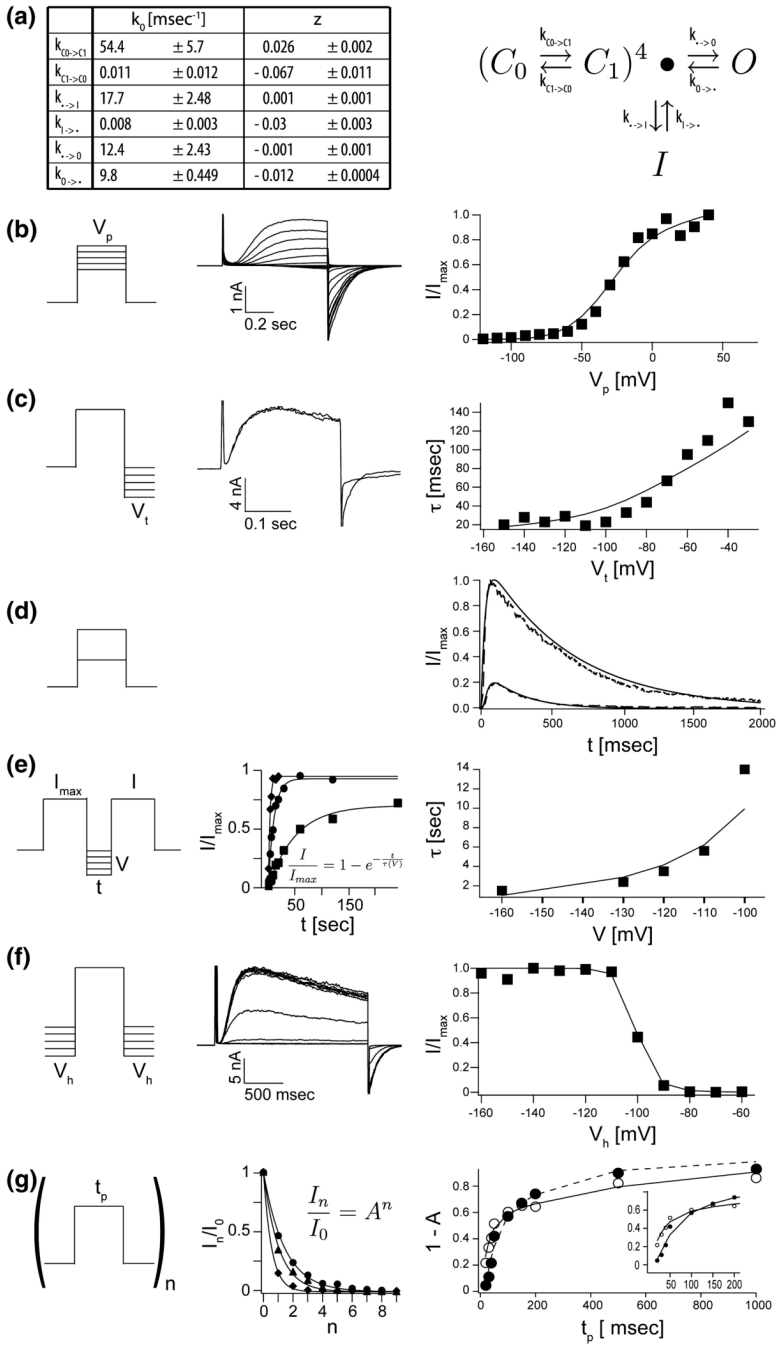

Figure 3. A detailed kinetic gating scheme for KvAP in DPhPC decane bilayers

A, The rate constants and their voltage dependences (± estimated standard deviations, see Materials and Methods) as derived from fitted data below for gating scheme (4) (see text). **B–G**, The solid lines in each right panel represent numerically modeled data using parameters from table **A**. Unless otherwise noted datapoints represent mean values of at least three independent measurements. **B**, G/V data: A representative family of currents is shown (middle panel) for voltage pulses from a common holding voltage (−120 mV) to increasingly more positive depolarization voltages (final +40 mV, ΔV 10 mV). Corresponding tail currents (I/I_{max}) are plotted (right panel). **C**, Voltage dependence of deactivation: Currents were elicited by stepping from a common holding voltage to a common depolarization voltage. Open

channels were closed (deactivated) by stepping back to increasingly negative hyperpolarization voltages (−30 mV to −150 mV, ΔV 10 mV). Two representative examples are shown, −50 mV and −140 mV. Tail currents were to fitted single exponential functions and the fitted values for τ were plotted as a function hyperpolarization voltage (right panel, n = 1). **D**, Fractional current response (I/I_{max} , dotted lines) after prolonged depolarization to +20 mV and +100 mV respectively. **E**, Recovery from inactivation: Paired 200 ms depolarization pulses to +100 mV with increasing interpulse length were used to determine the fractional recovery of channel activity (I/I_{max}) at different holding voltages (−100 mV to −160 mV) during the interpulse. All channels were completely inactivated at the end of the first of the paired pulses. The fractional recovered currents are plotted as a function of interpulse length (representative examples, middle panel) and fitted to single exponential functions. The fitted values for τ are plotted as a function of interpulse holding voltage (right panel). **F**, Steady State inactivation: From increasingly more negative holding voltages (−60 mV to 160 mV, ΔV 10 mV), currents were elicited by stepping to a common depolarization voltage. Representative recordings are shown (middle panel). Fractional elicited currents (I/I_{max}) are plotted as a function of holding voltage (right panel). **G**, Repetitive pulse of varying length t_p from a holding potential of −120 mV to +20 mV or +100 mV. Exemplary data for the fractional decrease in peak current I/I_{max} during depolarization as function of number of pulses (n) is shown (middle panel) for pulses to +20 mV and three different pulse lengths (20, 30 and 50 ms). The solid line represents a fit to $I/I_{max} = A^n$. The fraction of inactivated channel $1 – A$ is plotted against pulse length t_p for depolarization pulse to +20 mV (closed circles) and +100 mV (open circles).

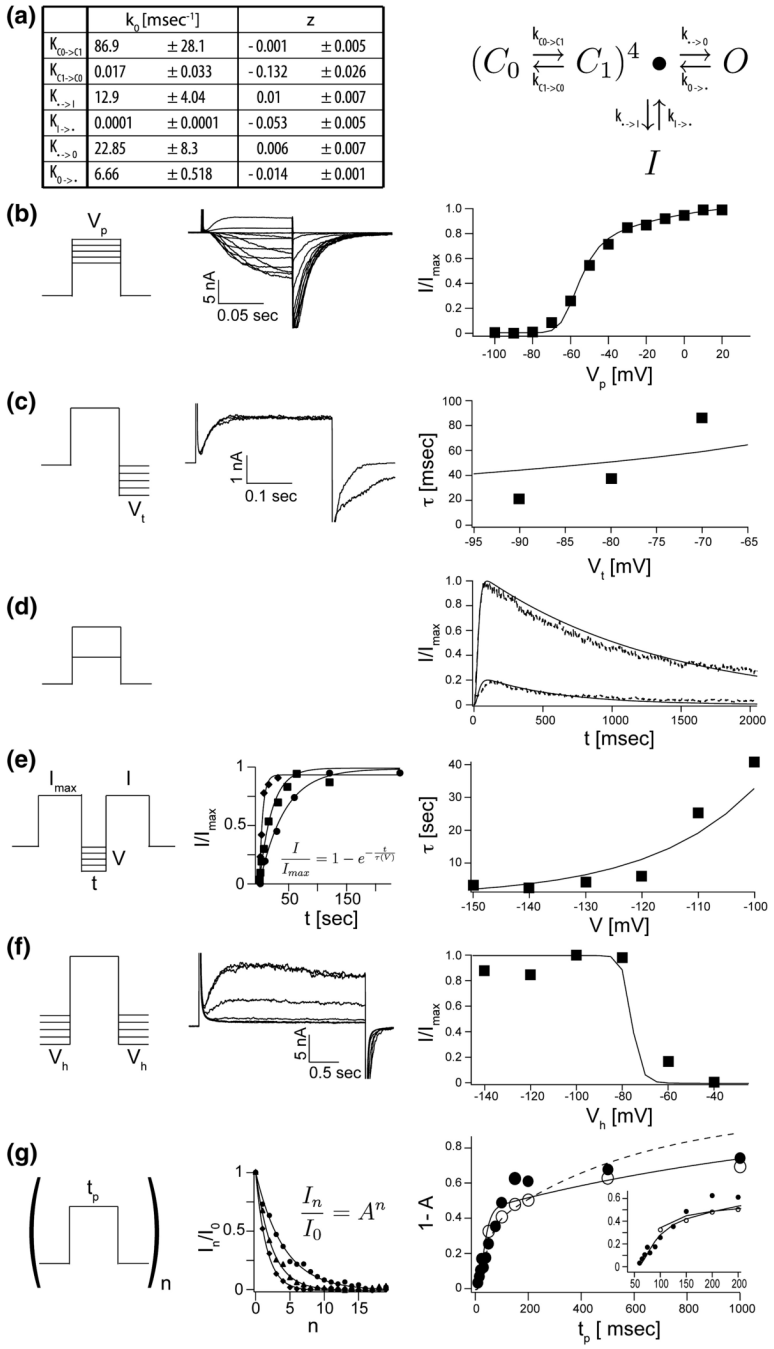

Figure 4. A detailed kinetic gating scheme for KvAP in POPE:POPG

A, The rate constants an their voltage dependences (± estimated standard deviations, see Materials and Methods) as derived from fitted data below for gating scheme (4) (see text). **B–G**, The solid lines in each right panel represent numerically modeled data using parameters from table **A**. Unless otherwise noted datapoints represent mean values of at least three independent measurements. **B**, G/V data: A representative family of currents is shown (middle panel) for voltage pulses from a common holding voltage (−100 mV) to increasingly more positive depolarization voltages (final +20 mV, ΔV 10 mV). Corresponding tail currents (I/I_{max}) are plotted (right panel). **C**, Voltage dependence of deactivation: Currents were elicited by stepping from a common holding voltage to a common depolarization voltage. KvAP

channels were closed (deactivated) by stepping back to increasingly negative hyperpolarization voltages (−60 mV to −160 mV, ΔV 10 mV). Two representative examples are shown (middle panel). Tail currents were fitted single exponential functions and the fitted values for τ plotted as a function hyperpolarization voltage (right panel, n = 1). **D**, Fractional current response (I/I_{max}, dotted line) after prolonged depolarization to +20 mV and +100 mV respectively. **E**, Recovery from inactivation: Paired 200 ms depolarization pulses to +100 mV with increasing interpulse length were used to determine the fractional recovery of channel activity (I/I_{max}) at different holding voltage (−100 mV to −150 mV, ΔV 10 mV) during the interpulse. All channels were completely inactivated at the end of the first of the paired pulses. The fractional recovered currents are plotted as a function of interpulse length (representative examples, middle panel) a fitted to single exponential functions. The fitted values for τ are plotted as a function of interpulse holding voltage (right panel). **F**, Steady State inactivation: From increasingly more negative holding voltages (−40 mV to 140 mV, ΔV 20 mV), currents were elicited by stepping to a common depolarization voltage. Representative recordings are shown (middle panel). Fractional elicited current (I/I_{max}) are plotted as a function of holding voltage (right panel). **G**, Repetitive pulse of varying length t_p from a holding potential of −100 mV to +20 mV or +100 mV. Exemplary data for the fractional decrease in peak current I/I_{max} during depolarization as function of number of pulses (n) is shown (middle panel) for pulses to +100 mV and three different pulse lengths (100, 150 and 200 ms). The solid line represents a fit to $I/I_{max} = A^n$. The fraction of inactivated channel $1 - A$ is plotted (right panel) against pulse length t_p for depolarization pulse to +20 mV (closed circles) and +100 mV (open circles).

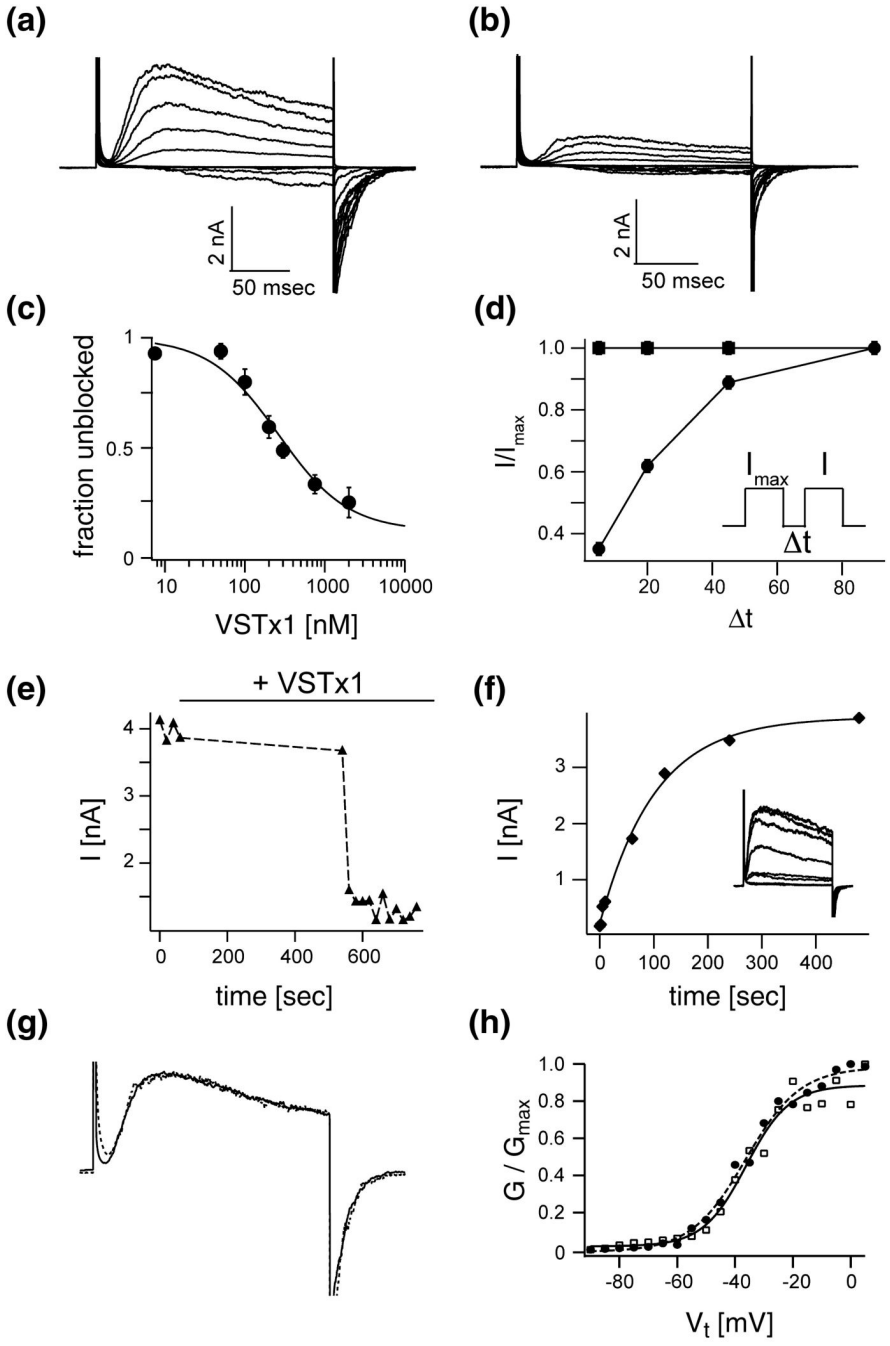

Figure 5. Voltage sensor toxin VSTx1 and nature of the inactivated state

All shown data was recorded with KvAP in the DPhPC decane bilayer system. Families of currents before (**A**) and after (**B**) the addition of 500 nM of VSTx1. Voltage pulses: −120 mV to +100 mV, ΔV 20 mV, interpulse length 20 seconds. **C**, VSTx1 affinity titration: Fraction of unblocked current I/I_{max} (mean ± s.e.m, n = 3) is graphed as a function of log(VSTx1 concentration). Voltage pulses: −120 mV to +100 mV, interpulse length 20 seconds. The solid line represents a fit to the titration data with $F_u = [1+[VSTx1]/K_D]^{-1}$ with K_D = 346 ± 51 nM. **D**, The fractional unblocked current I/I_{max} in a paired pulse experiment (mean ± s.e.m, n = 3) is plotted with (filled circles) and without (filled squares) 500 nM VSTx1 present as a function of interpulse length. As the interpulse length increases the fraction of unblocked current

increase, indicating an apparently decreased toxin affinity. **E**, VSTx1 is state dependent: Voltage pulse from −120 mV to +100 mV were elicited every 20 seconds. As the bilayer is held at −120 mV, 1 μM VSTx1 was added to the extracellular side of the channel. After a waiting period of 8 minutes without pulsing the above voltage protocols was resumed at an interpulse sequence of 20 seconds. During the hyperpolarized period no channel were blocked by VSTx1. Toxin block came on very rapidly after successive bilayer depolarizations. **F**, VSTx1 block can be overcome by prolonged hyperpolarization: Channels from **E** are blocked by addition of 1 μM VSTx1. Paired depolarization pulses with increasing interpulse length were used to determine the fractional recovery of channel activity by hyperpolarization. All channels were completely inactivated at the end of the first of the paired pulses by a set of 4 post train pulses. The fractional recovered currents are plotted as a function of interpulse length (representative example, inset) and fit to single exponential function (solid line). **G**, Normalized currents for pulses from −120 mV to +100 mV from families in **A** & **B** before (solid line) and after (dotted line) addition of 500 nM VSTx1. **H**, Boltzmann functions fit data from **A** (filled circles) with $V_{0.5}$ (mV) and Z: −36.4 ± 1, 9.5 ± 0.9 and data from **B** (open squares): −36.2 ± 1.5, 7.4 ± 1.35.